

Magnetic resonance imaging of laser polarized liquid xenon

C. H. Tseng,^{1,2} R. W. Mair,¹ G. P. Wong,¹ D. Williamson,³ D. G. Cory,² and R. L. Walsworth¹

¹Harvard-Smithsonian Center for Astrophysics, Cambridge, Massachusetts 02138

²Department of Nuclear Engineering, Massachusetts Institute of Technology, Cambridge, Massachusetts 02139

³Department of Radiology, Brigham and Women's Hospital, Boston, Massachusetts 02115

(Received 5 August 1998)

We demonstrate magnetic resonance imaging (MRI) of laser polarized liquid xenon, and image exchange between the liquid and vapor phases. The exceptionally large magnetization density of this liquid should allow MRI with micron-scale spatial resolution without signal averaging. Applications may include imaging of density equilibration and convective flow near xenon's liquid-vapor critical point, low-field imaging of porous media microstructure, and mapping of the dynamics of two-phase (liquid-gas) flows.

[S1063-651X(99)05602-0]

PACS number(s): 61.25.Bi, 76.60.Pc, 64.70.Fx

Xenon is unique among the noble gases, remaining liquid near room temperature: its liquid-vapor critical point is at ~ 290 K and 58 atm, and its solid-liquid-vapor triple point is at ~ 161 K and 0.8 atm. Liquid xenon has been employed in a variety of fundamental scientific investigations. For example, light scattering experiments near xenon's critical point have served as powerful probes of universal phenomena such as the range and lifetime of order parameter fluctuations [1], as well as the "critical slowing down" of diffusive and dissipative processes [2].

Xenon is nearly inert chemically, but because of the xenon atom's large electric polarizability the liquid is an excellent solvent—particularly for aliphatic materials. For example, hexadecane, benzene, toluene, hexane, and dodecane all have solubilities $> 10\%$ in liquid xenon at $\sim 0^\circ\text{C}$ [3]. In addition, nuclear magnetic resonance (NMR) studies of the spin- $\frac{1}{2}$ ^{129}Xe isotope have measured a relatively constant spin polarization lifetime (T_1) of ~ 25 min [4,5] and a relatively long spin decoherence time (T_2) > 1 s throughout the liquid xenon phase diagram [6], to within a few millikelvin of the critical point [7,8], and into the supercritical regime [9]. Thus liquid xenon approaches the behavior of an ideal, inert, NMR-detectable solvent.

Recently, Sauer, Fitzgerald, and Happer created *laser polarized* liquid xenon [5] by condensation of laser polarized xenon gas (i.e., gas with the ^{129}Xe component nuclear spin polarized via spin-exchange optical pumping [10]). Laser polarized liquid xenon can have a very large magnetization density, approximately 10^3 times greater than that of thermally polarized liquids such as water in magnetic fields of a few tesla. This exceptionally large magnetization density enables a variety of interesting scientific and technical applications, including: enhancement of the nuclear spin polarization of molecules dissolved in liquid xenon [11] (e.g., to aid NMR molecular spectroscopy and quantum computing); efficient transport and storage of polarized xenon for use in gas phase magnetic resonance imaging (MRI) [5]; and, as reported in this paper, high resolution MRI of liquid xenon and imaging of chemical exchange between the xenon liquid and vapor phases. With further development, laser polarized liquid xenon MRI may allow imaging of density equilibration and convective flow near xenon's liquid-vapor critical point,

low-field imaging of porous media microstructure, and mapping of the dynamics of two-phase (liquid-gas) flows.

(Note: NMR techniques have been used previously to study laser polarized liquid ^3He and its vapor [12] and liquid ^3He - ^4He mixtures [13], at cryogenic temperatures ~ 1 K. This work shows that one can distinguish between the NMR response of liquid and vapor phases, as well as obtain useful information about the geometry of the liquid phase and interphase dynamics [14]. In addition, three-dimensional gradient NMR techniques have been used to investigate the flow of liquid ^3He - ^4He mixtures in complex geometries [15].)

As a demonstration, we performed MRI on a drop of ~ 50 mm³ of laser polarized liquid xenon residing in the corner of a closed cylindrical Pyrex cell of ~ 25 cm³ volume [see Fig. 1(a)]. A complimentary image of the laser polarized xenon vapor filling the remainder of the Pyrex cell is shown in Fig. 1(b). Laser polarized liquid xenon was created by condensation of 80 atm·cm³ of xenon gas with an enriched abundance (90%) of the ^{129}Xe isotope, and a ^{129}Xe nuclear spin polarization of $\sim 5\%$ induced by standard spin-exchange optical pumping techniques [10]. The Pyrex cell was held in an iso-octane slush bath at 166 K [16], near the liquid xenon boiling point with an associated xenon vapor pressure of ~ 1 atm. The evaporation lifetime for the liquid xenon drop was comparable to the spin polarization lifetime (~ 25 min) and much longer than the time needed to acquire a magnetic resonance image (~ 10 s).

The images shown in Fig. 1 were obtained using a 4.7 T GE Omega/CSI spectrometer/imager operating at 55.3 MHz for ^{129}Xe using a homebuilt solenoid RF coil. Standard non-slice-selective fast gradient echo techniques were used for acquiring the laser polarized xenon images. The magnetic field gradient coils of the Omega instrument provide a maximum gradient strength of only 7 G/cm, which significantly limits the achievable MRI spatial resolution, even for laser polarized liquid xenon with its very large magnetization density [17]. Thus using the Omega's maximum gradient strength, we obtained a two-dimensional spatial resolution of 195×195 μm for the liquid xenon image in Fig. 1(a). Diffusive atomic exchange between the xenon vapor and liquid can also be inferred from the image in Fig. 1(b). This image was acquired with RF pulses exciting only the vapor reso-

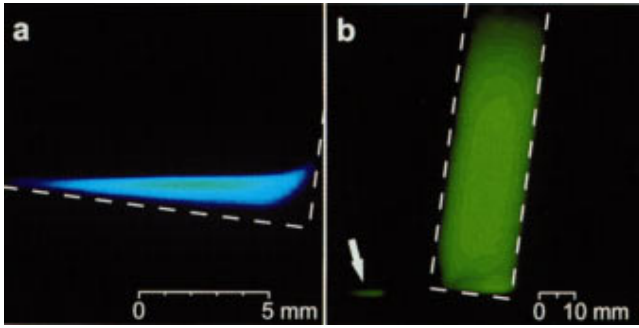


FIG. 1. (Color) (a) Magnetic resonance image of a laser polarized liquid xenon drop at 166 K in the corner of a tilted Pyrex cell. Image resolution is $195 \times 195 \mu\text{m}$ (limited by magnetic field gradients provided by the MRI instrument). (b) Complimentary image of laser polarized xenon vapor above the liquid drop. Image resolution is $860 \times 860 \mu\text{m}$. Note the physically displaced “ghost” image of the liquid drop, highlighted by an arrow, resulting from RF-excited vapor atoms condensing into the liquid phase before signal acquisition. The bottom of the vapor image distorts slightly due to the magnetic susceptibility difference between the vapor and liquid, as well as the large dipolar magnetic field created by the polarized liquid xenon drop. The xenon images were acquired using fast low-flip-angle-excitation gradient echo sequences with chemical-shift but non-slice-selective RF pulses. The RF pulse flip angle was nominally 12° . For the liquid image, a data matrix of 128×64 points was acquired, the field of view (FOV) was $25 \times 12.5 \text{ mm}$, the echo time (TE) was 15.5 ms, and the scan repetition time (TR) was 150 ms. For the vapor image, the data matrix was 128×128 , FOV = $110 \times 110 \text{ mm}$, TE = 10.5 ms, and TR = 150 ms. All images were obtained without signal averaging.

nance. However, sufficient xenon vapor atoms condensed into the liquid during the time to acquire a line of reciprocal or k space imaging data ($\sim 20 \text{ ms}$) that a significant NMR signal was produced at the liquid xenon frequency, and a “ghost” image of the liquid drop was created physically displaced from the vapor image. [The ghost liquid image is highlighted by an arrow in Fig. 1(b).] The displacement of the ghost image was caused by the large chemical shift ($\sim 250 \text{ ppm}$) between the NMR frequencies of the xenon vapor and liquid phases.

As discussed below, the larger imaging gradients available on MRI microscopy instruments ($\sim 100 - 2000 \text{ G/cm}$), should allow an imaging resolution of $\sim 10 \mu\text{m}^3$ for laser polarized liquid xenon *without signal averaging* [18]. Such resolution would be the highest achieved with MRI in any system [17,18], and would approach the resolution provided by optical microscopy.

The spatial resolution of an NMR image (Δx) is determined by the magnetic field gradients imposed on the sample to establish a magnetization grating of wave number k for each spatial dimension [$\Delta x \sim k^{-1} \sim (\text{gradient strength})^{-1}$] balanced against both the sample’s rate of spin decoherence, which obscures the phase of the magnetization grating, and atomic or molecular diffusion, which reduces the amplitude of the magnetization grating during data acquisition [17,18]. For example, in the absence of diffusion the one-dimensional image resolution set by a homogeneous spin decoherence time, T_2 , is $\Delta x = [(\gamma T_2/2) dB_z/dx]^{-1}$, where dB_z/dx is the applied imaging gradient in that dimension and γ is the sample’s gyromagnetic ratio in angular units. However, to real-

ize an effective NMR image of a particular spatial resolution there must also be a sufficient signal-to-noise ratio (SNR) in the imaging data [17,18]. Thus for a typical NMR sample such as water, for which the ^1H spin density is $\sim 0.7 \times 10^{11} \mu\text{m}^{-3}$, the thermal Boltzmann spin polarization near room temperature is $\sim 4 \times 10^{-6}$ per tesla, and the single acquisition NMR detection sensitivity is $\sim 10^{15}$ ^1H spins, a three-dimensional imaging resolution of less than $\sim 1000 \mu\text{m}^3$ requires extensive data acquisition, often lasting many hours. In contrast, the exceptionally large magnetization density of laser polarized liquid xenon should enable greater imaging resolution for a given data acquisition time.

To estimate the ultimate resolution of laser polarized liquid xenon MRI, one must quantify the liquid xenon magnetization density, the spin decoherence time (T_2) and the atomic self-diffusion coefficient [17,18]. [We assume here that the liquid xenon sample is homogeneous and well separated from materials of differing magnetic susceptibility.] At 4.7 T we measured the NMR SNR per unit volume of laser polarized liquid xenon at 166 K to be approximately a hundred times greater than that of liquid water, a result that is consistent with the samples’ spin polarizations ($\sim 5\%$ for ^{129}Xe and 0.002% for ^1H), relative spin densities ($1.2 \times 10^{22} \text{ cm}^{-3}$ for ^{129}Xe [19] and $6.7 \times 10^{22} \text{ cm}^{-3}$ for ^1H), and different gyromagnetic ratios (11.8 MHz/T for ^{129}Xe and 42.6 MHz/T for ^1H). We also measured the T_2 of laser polarized liquid xenon to be longer than one second at 4.7 T and 166 K using the CPMG method of multiply-refocused spin echoes [20], a result that is consistent with past work [6]. Finally, the self-diffusion coefficient of liquid xenon has previously been determined using thermally polarized xenon to be $3.9 \times 10^{-9} \text{ m}^2 \text{ s}^{-1}$ at 166 K [6].

With knowledge of these parameters, one can apply well-established MRI principles [17,18] and estimate the ultimate three-dimensional spatial resolution of laser polarized liquid xenon MRI with no signal averaging to be $\sim 10 \mu\text{m}^3$ at low temperatures ($\sim 166 \text{ K}$), requiring imaging gradients of $\sim 400 \text{ G/cm}$.

The fast, ultrahigh resolution of laser polarized liquid xenon MRI may enable a variety of scientific and technical investigations. We discuss three examples here. First, this new imaging technique could be used to study the universal phenomenon of density equilibration in critical fluids. Recent theoretical work [21] indicates that when a near-critical fluid is exposed to an external perturbation such as a change in temperature of one end of the sample, an adiabatic equilibration mechanism known as the “piston effect” [22] induces transient boundary layers in the fluid density. For xenon within about one degree of its liquid-vapor critical point these density boundary layers are predicted to be $\sim 50 \mu\text{m}$ thick, to deviate by $\sim 2\%$ from the nominal density profile (a smooth gradient induced by gravity), and to persist for a few seconds [21]. Under certain nonequilibrium conditions, anomalously high density in the transient boundary layer may also induce convective flow in the critical fluid and significantly change the system’s dynamic behavior and transport properties. Laser polarized xenon MRI may be used to measure the density, thickness, and lifetime of such transient density boundary layers, and to image convective near-critical flow.

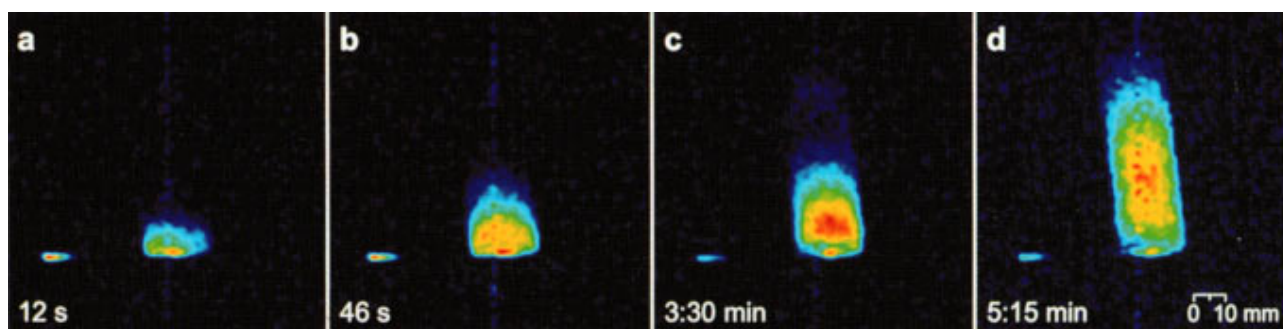


FIG. 2. (Color) Magnetic resonance images of the evaporation of laser polarized liquid xenon into the vapor. First, the magnetization of the xenon vapor was destroyed by application of multiple selective RF and magnetic field gradient pulses. (a)–(d) Xenon vapor images subsequent to the selective destruction of the vapor magnetization, showing xenon spins that have evaporated from the liquid and diffused into the vapor. The imaged propagation of laser polarized xenon vapor is consistent with the xenon gas diffusion coefficient at the sample's pressure and temperature: $\sim 2 \text{ mm}^2 \text{ s}^{-1}$. Images were obtained with the same technique and parameters as for Fig. 1(b), except for a nominal RF excitation flip angle of 8 degrees and a TR of 25 ms, giving a total acquisition time of 7 s for each image.

A second promising application of laser polarized xenon MRI is to investigate two-phase (liquid-gas) phenomena. As a demonstration, we imaged xenon spins evaporating from the liquid into the vapor (Fig. 2), as well as condensing from the vapor into the liquid (Fig. 3). These images were acquired using appropriate combinations of RF and magnetic field gradient pulses to selectively destroy the laser-polarization-produced magnetization in one phase (liquid or vapor), while leaving undisturbed the magnetization of the other phase. Sequential images were then acquired of the phase whose magnetization had been destroyed, showing the buildup of magnetization as polarized xenon atoms move between phases to re-establish equilibrium. The images in Figs. 2 and 3 represent the net transport of xenon magnetization due to three competing processes: (i) the slow boiling of the liquid xenon drop (lifetime $\sim 25 \text{ min}$); (ii) intraphase and interphase atomic diffusion; and (iii) depletion of the xenon magnetization by the acquisition of images. Extending these MRI techniques to flowing two-phase systems may allow the simultaneous mapping of dynamics in both phases. For example, the polarized-liquid-induced distortion of the xenon vapor image shown in Fig. 1(b) indicates an effective coupling between the liquid and vapor phases, which may enable measurement of the relative velocity field of a two-phase flow using multidimensional NMR correlation techniques [23].

Finally, we note a third promising application of laser polarized liquid xenon: serving as a probe of porous media microstructure using *low-field* MRI. Conventional, high-magnetic-field MRI of thermally polarized liquids infused in porous media (reservoir rocks, ceramics, etc.) suffers from large, local magnetic field gradients caused by the magnetic susceptibility difference between the solid grains and the infused liquid. These field gradients can be as high as 1000 G/cm at typical magnetic fields of a few tesla [24], and thus can severely degrade and distort images of the sample pore space. Operating at lower magnetic fields ($< 0.1 \text{ T}$) greatly reduces the effect of magnetic susceptibility gradients (which scale as the applied field squared); however, very low spin polarization makes micron-scale MRI of thermally polarized samples impractical at low magnetic fields. In contrast, the magnetization of a laser polarized sample is independent of the applied field strength, which enables practical low-field imaging. We recently demonstrated MRI of laser polarized ^3He gas at 21 gauss (with $\sim 1 \text{ mm}$ spatial resolution, limited by rapid gas diffusion), and showed the greatly reduced effects of magnetic susceptibility gradients [25]. Low-field MRI of infused laser polarized liquid xenon may provide direct visualization of porous microstructure on the micron scale, which at present is best inferred indirectly with NMR using pulsed-field-gradient diffusion measurements [26,27].

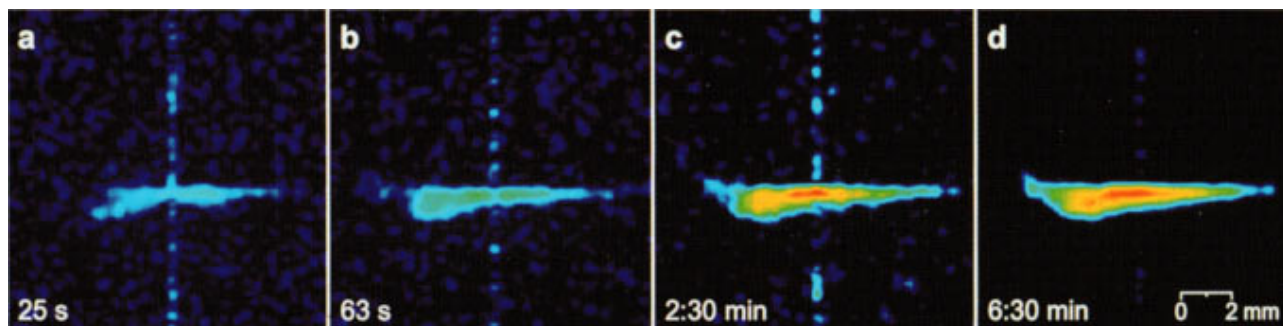


FIG. 3. (Color) Magnetic resonance images of the condensation of laser polarized xenon vapor into the liquid. First, the magnetization of the xenon liquid was destroyed by application of multiple selective RF and magnetic field gradient pulses. (a)–(d) Xenon liquid images subsequent to the selective destruction of the liquid magnetization, showing xenon spins that have condensed from the vapor and diffused into the liquid. Images were obtained with the same technique and parameters as for Fig. 1(a), except for a nominal RF excitation flip angle of 8° , a TE of 16.5 ms, and a TR of 100 ms, giving a total acquisition time of 14 s for each image.

In conclusion, we have demonstrated magnetic resonance imaging (MRI) of laser polarized liquid xenon, and imaged chemical exchange between the liquid and vapor phases. The exceptionally large magnetization density of this liquid should allow MRI with micron-scale spatial resolution without signal averaging. Applications may include imaging of density equilibration and convective flow near the liquid-vapor critical point, low-field imaging of porous media mi-

crostructure, and mapping of the dynamics of two-phase (liquid-gas) flows.

We gratefully acknowledge scientific discussions with Robert Gammon, Jeff Shaumeyer, and Horst Meyer, and technical assistance from Dominik Hoffmann. This work was supported by NSF Grant No. BES-9612237 and the Smithsonian Institution.

-
- [1] H. L. Swinney and D. L. Henry, *Phys. Rev. A* **8**, 2586 (1973); H. Guttinger and D. S. Cannell, *ibid.* **22**, 285 (1980).
- [2] I. W. Smith, M. Giglio, and G. B. Benedek, *Phys. Rev. Lett.* **27**, 1556 (1971).
- [3] P. M. Rentzepis and D. C. Douglass, *Nature (London)* **293**, 165 (1981); P. M. Rentzepis and D. C. Douglass (private communications).
- [4] E. R. Hunt and H. Y. Carr, *Phys. Rev.* **130**, 2302 (1963).
- [5] K. L. Sauer, R. J. Fitzgerald, and W. Happer, *Chem. Phys. Lett.* **277**, 153 (1997).
- [6] W. M. Yen and R. E. Norberg, *Phys. Rev.* **131**, 269 (1963).
- [7] L. M. Stacey, B. Pass, and H. Y. Carr, *Phys. Rev. Lett.* **23**, 1424 (1969).
- [8] R. S. Ehrlich and H. Y. Carr, *Phys. Rev. Lett.* **25**, 341 (1970).
- [9] M. Haake, B. M. Goodson, D. D. Laws, E. Brunner, M. C. Cyrier, R. H. Havlin, and A. Pines, *Chem. Phys. Lett.* **292**, 686 (1998).
- [10] T. G. Walker and W. Happer, *Rev. Mod. Phys.* **69**, 629 (1997).
- [11] R. J. Fitzgerald, K. L. Sauer, and W. Happer, *Chem. Phys. Lett.* **284**, 87 (1998).
- [12] G. Tastevin, P. J. Nacher, L. Wiesenfeld, M. Leduc, and F. Laloe, *J. Phys. (France)* **49**, 1 (1988).
- [13] G. Tastevin, *J. Low Temp. Phys.* **89**, 317 (1992).
- [14] G. Tastevin, *Physica B* **194-196**, 911 (1994).
- [15] D. Candela, M. E. Hayden, and P. J. Nacher, *Phys. Rev. Lett.* **73**, 2587 (1994).
- [16] R. E. Rondeau, *J. Chem. Eng. Data* **10**, 124 (1965).
- [17] P. T. Callaghan, *Principles of Nuclear Magnetic Resonance Microscopy* (Oxford, New York, 1991), Chap. 4, pp. 173 – 237.
- [18] S. Choi, X.-W. Tang, and D.G. Cory, *Int. J. Imaging Syst. Technol.* **8**, 263 (1997).
- [19] R. L. Streever and H. Y. Carr, *Phys. Rev.* **121**, 20 (1961).
- [20] H. Y. Carr and E. M. Purcell, *Phys. Rev.* **94**, 630 (1954); S. Meiboom and D. Gill, *Rev. Sci. Instrum.* **29**, 668 (1958).
- [21] H. Boukari, R. L. Pego, and R. W. Gammon, *Phys. Rev. E* **52**, 1614 (1995).
- [22] H. Boukari, M. E. Briggs, J. N. Shaumeyer, and R. W. Gammon, *Phys. Rev. Lett.* **65**, 2654 (1990); H. Boukari, J. N. Shaumeyer, M. E. Briggs, and R. W. Gammon, *Phys. Rev. A* **41**, 2260 (1990); A. Onuki, H. Hao, and R. A. Ferrell, *ibid.* **41**, 2256 (1990); A. Onuki and R. A. Ferrell, *Physica A* **164**, 245 (1990).
- [23] W. S. Warren, S. Lee, W. Richter, and S. Vathyam, *Chem. Phys. Lett.* **247**, 207 (1995).
- [24] M. D. Hurlimann, *J. Magn. Reson.* **131**, 232 (1998).
- [25] C-H. Tseng, G. P. Wong, V. R. Pomeroy, R. W. Mair, D. P. Hinton, D. Hoffmann, R. E. Stoner, F. W. Hersman, D. G. Cory, and R. L. Walsworth, *Phys. Rev. Lett.* **81**, 3785 (1998).
- [26] P. T. Callaghan, *Principles of Nuclear Magnetic Resonance Microscopy* (Oxford, New York, 1991), Ch. 6, pp 337–353; P. T. Callaghan, A. Coy, D. MacGowan, K. J. Packer, and F. O. Zelaya, *Nature (London)* **351**, 467 (1991).
- [27] P. P. Mitra, P. N. Sen, and L. M. Schwartz, *Phys. Rev. B* **47**, 8565 (1993); P. N. Sen, L. M. Schwartz, P. P. Mitra, and B. I. Halperin, *ibid.* **49**, 215 (1994); L. L. Latour, P. Mitra, R. L. Kleinberg, and C. H. Sotak, *J. Magn. Reson., Ser. A* **101**, 342 (1993).